CrossMark
click for updates

Novel UIO-66-NO$_2$@XC-72 nanohybrid as an electrode material for simultaneous detection of ascorbic acid, dopamine and uric acid†

Wanqing Zhang,[ab] Jun Chen,[b] Yuanchao Li,[b] Wenxiang Yang,[b] Yadong Zhang[*a] and Yuping Zhang[*b]

UIO-66-NO$_2$@XC-72 nanohybrid was synthesized from UIO-66-NO$_2$ via hydrothermal synthesis method, followed by mixing with XC-72 carbon (XC-72). The compositions, microstructures, textural parameters and morphologies of the resulting nanomaterials were characterized by FTIR, XRD, N$_2$ adsorption–desorption, SEM and TEM. The UIO-66-NO$_2$@XC-72-modified glassy carbon electrode (GCE) sensor was successfully applied to the simultaneous determination of ascorbic acid (AA), dopamine (DA) and uric acid (UA). Owing to the large surface area of UIO-66-NO$_2$ and good conductivity of XC-72, as well as the hydrogen bond effect between the UIO-66-NO$_2$ and the analyte, the proposed sensor exhibited excellent linear responses to AA, DA and UA under optimized conditions. The detection ranges were 0.2–3.5 μM for AA, 0.03–2.0 μM for DA and 0.75–22 μM for UA, with the detection limits (S/N = 3) of 0.12 μM, 0.005 μM and 0.03 μM, respectively. Moreover, the high reproducibility and stability of the sensor were obtained in all the experiments. The sensor was also successfully applied to the determination of DA in hydrochloride injection solution and UA in urine sample. The MOFs@XC-72 would be potentially applied as a modified electrode sensor material for the determination of other small biomolecules.

1. Introduction

Ascorbic acid (AA), dopamine (DA) and uric acid (UA) usually coexist in human metabolism, renal and central nervous systems, playing important roles in real biological matrixes.[1–5] The development of a sensitive and selective method for simultaneous detection of the three small biomolecules is therefore desirable.[1,2,5] Electrochemical method possesses the advantages of rapidity, economy, convenience and sensitivity, combined with the high electrochemical activity of AA, DA and UA, thus it is usually adopted to detect the three species.[3,4,6] However, the oxidation peaks of the three compounds are broad and overlap using an unmodified electrode. To date, there have been considerable efforts devoted to developing electrode sensor modifiers to promote the electron transfer and achieve high sensitivity and selectivity,[7,8] such as carbon nanotubes,[9–11] noble metals nanoparticles,[12–16] mesoporous carbons,[17] conductive polymers,[3,18–21] and hybrids.[22,23]

Recently, metal–organic frameworks (MOFs) have attracted much attention as electrochemical sensor materials for their rich structure types, high surface area, tunable pores and various functionalities.[24–29] Nevertheless, most MOFs have the major drawback of their poor stability, which are derived from the reversible nature of the coordination bonds.[24,30] Moreover, nano-scale MOFs have more potential applications because they exhibit much higher surface areas, uniform sizes, well-defined functionality, and stable dispersions.[31,32] However, numerous of synthesized MOFs are ascribed to the micron-sized materials, resulting in the weakened adhesion properties between MOFs and glassy carbon electrode (GCE). Furthermore, plenty of MOFs belong to poor electrical conductors.[27,33,34] To overcome these problems, many nanostructured and conductive MOFs were synthesized and applied in sensors fields.[35–37] For poor electron-conductive MOFs, an efficient method is to mix MOFs with conductive materials. UIO-66-R (–H, –NO$_2$, –NH$_2$) were of great interest due to their large surface area, good stability and unique functional groups.[38–40] The applications of UIO-66-NO$_2$ and UIO-66-NH$_2$ as catalytic materials were related to the special functional groups, which can easily interact with the analyte, such as hydrogen bond effect, electrostatic effect. Besides, the band gap value (E_g) of UIO-66-R is a very important parameter for electrochemical reaction at sensors.[41] According to the theoretical calculations and experiments, the E_g value of UIO-66-R decreased in the following order: –H > –NO$_2$ > –NH$_2$.[42] Therefore, nano-UIO-66-NO$_2$ was selected to be modified electrode sensors materials. To enhance the conductivity of the nanohybrid, the conductive XC-72 was mixed with the

[a]School of Chemical Engineering and Energy, Zhengzhou University, Zhengzhou 450001, China. E-mail: zhangydzzu@163.com

[b]School of Chemistry and Chemical Engineering, Henan Institute of Science and Technology, Xinxiang, 453003, China. E-mail: bejing2008zyp@163.com

† Electronic supplementary information (ESI) available. See DOI: 10.1039/c6ra26933h

MOFs.[26,43] However, there are a few literatures about UIO-66-NO_2@XC-72 to determine AA, DA and UA.

Herein, we provide a strategy to prepare UIO-66-NO_2 *via* hydrothermal synthesis method, followed by mixing with XC-72. When the hybrid was applied to modify the GCE, it was used to simultaneously detect the three compounds. Three well-defined separated peaks were observed by using cyclic voltammetry (CV) and differential pulse voltammetry (DPV) methods. Furthermore, the developed sensor exhibited high sensitivity, selectivity, reproducibility and stability. Besides, the sensor was also suitable to detect the real samples. The wide linear range and low detection limits for the three species were obtained due to the synergistic effect of UIO-66-NO_2 and XC-72.

2. Experimental

2.1 Chemicals and apparatus

Zirconium chloride ($ZrCl_4$), 2-nitroterephthalic acid (H_2BDC-NO_2) and *N,N*-dimethylformamide (DMF) were purchased from Aldrich. AA, DA and UA were obtained from Alfa Aesar and XC-72 carbon from Cabot Carbon Corporation (USA). Sodium dihydrogen phosphate (NaH_2PO_4) and disodium hydrogen phosphate (Na_2HPO_4) were bought from Aldrich. Phosphate buffer solutions (PBS, 0.1 M) were prepared from stock solutions of 0.1 M NaH_2PO_4, Na_2HPO_4 and H_3PO_4. All other reagents were at least analytical grade.

2.2 Preparation of UIO-66-NO_2

The UIO-66-NO_2 was prepared according to the reported method.[44] Briefly, $ZrCl_4$ (0.932 g), H_2BDC-NO_2 (0.845 g) and 0.67 mL concentrated HCl were added in 10 mL DMF in a Teflon-lined stainless steel autoclave, followed by ultrasonic treatment 5 min. The autoclave was placed in an oven at 120 °C for 16 h, and the mixture was filtered and washed with DMF and acetone, respectively. The final product was activated at 60 °C under a vacuum drying for 10 h.

2.3 Fabrication of modified GCE sensors

Prior to preparation procedure, the GCE was carefully polished with 0.1 and 0.05 μm Al_2O_3 power. Afterwards, the electrode was sonicated in nitric acid solution ($HNO_3 : H_2O = 1 : 1$), acetone, and double distilled water, and then it was allowed to dry at room temperature. 5.0 mg of the individual samples (UIO-66-NO_2, XC-72) or the mixed samples (the ratio of UIO-66-NO_2 and XC-72 was 1 : 5, 1 : 6, 1 : 7, 1 : 8, 1 : 9, 1 : 10) were dispersed in 5 mL H_2O followed by sonication for 30 min. The modified electrode sensors were prepared by casting 5 μL of the suspension on GCE surface, and dried under an infrared lamp (Scheme 1).

2.4 Apparatus and instruments

FTIR spectrum was recorded on a Lambda 7600. Power X-ray diffraction (XRD) data were collected on a DX-2700B diffractometer. N_2 adsorption–desorption isotherms were carried out by using a BeiShiDe Instrument-S&T. The morphologies were examined using a Quanta 200 scanning electron microscope and an H-7500 transmission electron microscope.

The cyclic voltammetry (CV), differential pulse voltammetry (DPV) measurements and electrochemical impedance spectroscopy (EIS) characterizations were performed on a Shiruisi electrochemical workstation. A conventional three electrode system was used in the measurements composed of a platinum wire counter electrode, a saturated calomel reference electrode (SCE), and a bare or modified glassy carbon working electrode.
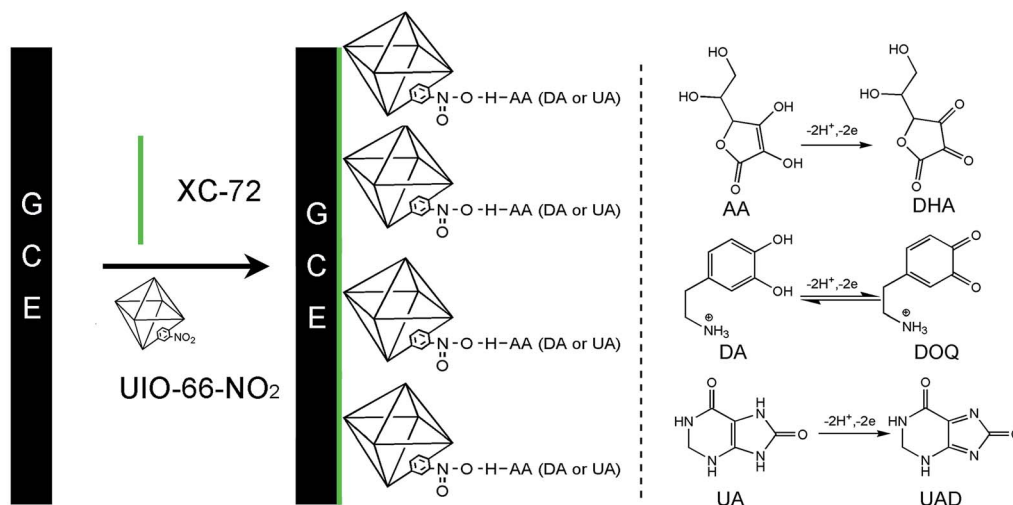
AA represents ascorbic acid, DA represents dopamine, UA represents uric acid, DHA represents Dehydro ascorbate, DOQ represents Dopaquinone, and UAD represents Uric acid 4,5 diol.

Scheme 1 The modified electrode sensor preparation process and the redox reaction mechanism of AA, DA and UA at UIO-66-NO_2@XC-72/GCE sensor.

Table 1 Porous textural parameters of the UIO-66-NO$_2$, XC-72 and UIO-66-NO$_2$@XC-72

Samples	$S_{Langmuir}$/ m^2 g^{-1}	S_{BET}/ m^2 g^{-1}	Micropore volume/ cm^3 g^{-1}	Average pore diameter/ nm
UIO-66-NO$_2$	978	865	0.14	3.01
XC-72	324	213	0.03	14.3
UIO-66-NO$_2$@XC-72	644	528	0.06	13.0

3. Results and discussion

3.1 Physical characterization

Fig. S1† shows the FTIR spectrum of UIO-66-NO$_2$. The absorption peaks at 3439 cm^{-1}, 1658 cm^{-1}, 1550 cm^{-1}, and 1380 cm^{-1} should belong to –OH stretching vibration, –C=O vibration peak, –NO$_2$ asymmetric stretching and symmetric stretching peaks, respectively.[24] The XRD pattern of as-synthesized UIO-66-NO$_2$ matches well with the simulated one, demonstrating the successful preparation of UIO-66-NO$_2$.[24,25] For XC-72 sample, the broad peak at $2\theta = 24.6°$ is corresponding to the (0 0 2) peak of the hexagonal structure of graphitic structure.[45] Besides, the UIO-66-NO$_2$@XC-72 displays the characteristic diffraction peaks of both UIO-66-NO$_2$ and XC-72, endowing the modified electrode sensor with synergistic advantages of the two materials (Fig. S2†).

Fig. S3a† reveals that all samples are typical characteristic of the microporous materials because they possess reversible, type-I isotherms with no obvious hysteresis.[44,46] The pore size distributions (PSD) show the predominant pore size of the three samples from 0.49 nm for UIO-66-NO$_2$, 0.43 nm for XC-72 to 0.45 nm for UIO-66-NO$_2$@XC-72 (Fig. S3b†). Table 1 summarizes the Langmuir surface area, BET, micropore volume and average pore diameter data of UIO-66-NO$_2$, XC-72 and UIO-66-NO$_2$@XC-72. It can be seen that UIO-66-NO$_2$@XC-72 exhibits the smaller surface area, micropore volumes and larger pore diameter compared with UIO-66-NO$_2$ material. The results indicate that UIO-66-NO$_2$ is successfully mixed with XC-72.

Fig. 1(a and d) show that the UIO-66-NO$_2$ possesses nanometre scale particles with the sizes of about 150 nm. The XC-72

Fig. 1 SEM and TEM images of UIO-66-NO$_2$ (a and d), XC-72 (b and e) and UIO-66-NO$_2$@XC-72 (c and f). Ratio of UIO-66-NO$_2$ and XC-72 was 1 : 6 in UIO-66-NO$_2$@XC-72.

displays spherical particles with the sizes of less than 100 nm in Fig. 1(b and e). Fig. 1(c and f) reveal that the UIO-66-NO$_2$ is well-dispersed over XC-72 and its main morphology is not destroyed for UIO-66-NO$_2$@XC-72.

3.2 Electrochemical characterization

The CV curves and EIS of the bare GCE and the different sensors are recorded in Fig. 2. The peak potential separation (ΔE_p) reflects the electron transfer rate for the CV responses.[47] As shown in Fig. 2a, the bare electrode has a pair of reversible redox peaks ($i_{pa} = 24.98$ µA, $i_{pc} = -21.58$ µA, $\Delta E_p = 0.18$ V), while the UIO-66-NO$_2$/GCE sensor exhibits a broadened peak potential and small peak current, suggesting that the sensor surface is blocked due to the poor electron transfer of UIO-66-NO$_2$ material.[48] When XC-72 and UIO-66-NO$_2$@XC-72 modified electrode surface, the ΔE_p values decline to 0.16 and 0.15 V, respectively. The XC-72/GCE ($i_{pa} = 32.88$ µA, $i_{pc} = -31.11$ µA) and UIO-66-NO$_2$@XC-72/GCE sensors ($i_{pa} = 30.65$ µA, $i_{pc} = -29.81$ µA) possess higher current, and smaller ΔE_p profiles, indicating that XC-72 possesses good electronic conductivity and is beneficial to electron transfer.[48–50] When 5.0 mM Ru(NH$_3$)$_6$Cl$_3$ was added into 0.1 M KCl solution, the similar results can be obtained from Fig. 2b. It can be seen that the UIO-66-NO$_2$/GCE sensor exhibits a broadened peak, while the XC-72/GCE ($i_{pa} = 37.67$ µA, $i_{pc} = -27.95$ µA, $\Delta E_p = 0.15$ V) and UIO-66-NO$_2$@XC-72/GCE ($i_{pa} = 34.81$ µA, $i_{pc} = -23.59$ µA, $\Delta E_p = 0.16$ V) sensors receive higher current and similar ΔE_p value compare with bare electrode ($i_{pa} = 20.41$ µA, $i_{pc} = -12.59$ µA, $\Delta E_p = 0.16$ V). The results confirm XC-72/GCE and UIO-66-NO$_2$@XC-72/GCE sensors have better electrochemical properties than UIO-66-NO$_2$/GCE.

It is also investigated by EIS measurements that the electron transfer kinetics occur at the interface of electrode/electrolyte (Fig. 2c).[51] The distinct semicircle curve at high frequencies reflects the ability of electron transfer (R_{ct}) of different sensors[47,48] and the smaller diameter of R_{ct} represents higher electron transfer at the interface of electrode/electrolyte.[49,52] The R_{ct} values increase in the order of the XC-72/GCE sensor < UIO-66-NO$_2$@XC-72/GCE sensor < bare GCE < UIO-66-NO$_2$/GCE sensor. It reveals that the conductivity and electrochemical properties are well improved at XC-72 and UIO-66-NO$_2$@XC-72 modified electrode sensor. The results are consistent with our data obtained by CV.

3.3 Electrocatalytic oxidation of AA, DA and UA

Fig. 3a depicts the three individual and mixed oxidation peaks at the potentials of 0.015 V, 0.23 V and 0.38 V at the UIO-66-NO$_2$@XC-72/GCE sensor, corresponding to AA, DA and UA, respectively. Fig. 3b shows the CVs responses of the ternary mixture of AA, DA and UA at different electrodes. For bare GCE, the oxidation peaks of the three species nearly overlapped and a broad peak was found at 0.5 V, proving that it possessed poor sensitivity and selectivity towards the oxidation of the three compounds. For comparison, the UIO-66-NO$_2$/GCE sensor had no obvious redox peaks and possessed a large background current due to the weak conductivity of the MOFs. For XC-72/
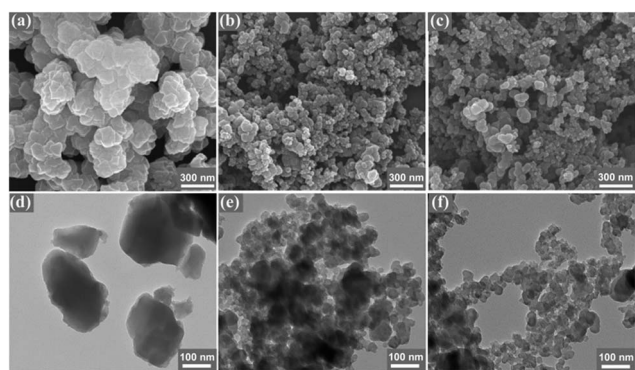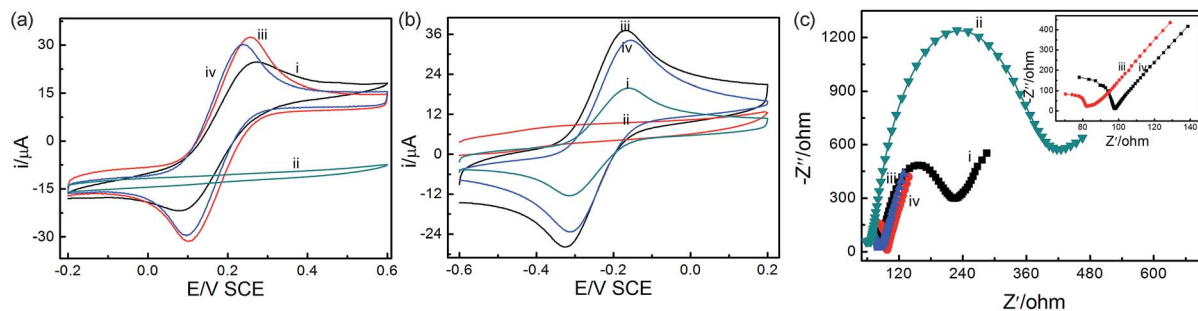
Fig. 2 The cyclic voltammetry (CV) curves of bare GCE (i), UIO-66-NO$_2$/GCE (ii), XC-72/GCE (iii) and UIO-66-NO$_2$@XC-72/GCE (iv) sensors in (a) 5 mM K$_3$[Fe(CN)$_6$]/K$_4$[Fe(CN)$_6$] solution, (b) 5 mM Ru(NH$_3$)$_6$Cl$_3$ solution containing 0.1 mM KCl as supporting electrolyte. (c) Electrochemical impedance spectroscopy (EIS) of the different electrode sensors in 5 mM K$_3$[Fe(CN)$_6$]/K$_4$[Fe(CN)$_6$] solution with 0.1 mM KCl. Scan rate: 100 mV s^{-1}.
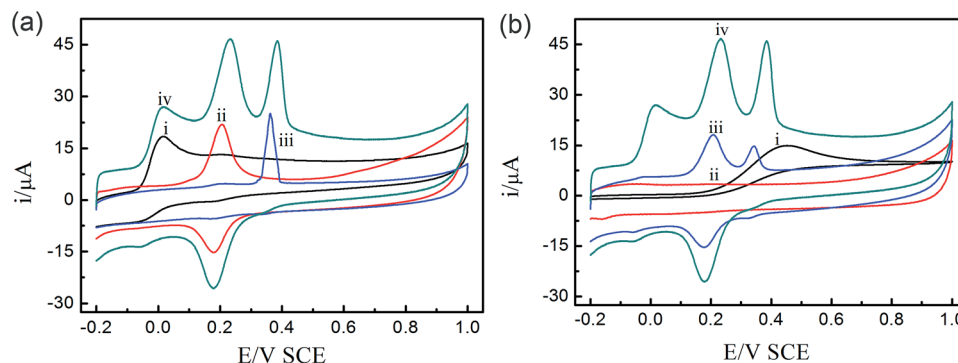

Fig. 3 (a) CVs of (a) 3 μM AA (i), 1.5 μM DA (ii), 1.5 μM UA (iii) and the mixture of AA (3 μM), DA (1.5 μM) and UA (1.5 μM) (iv), respectively at UIO-66-NO$_2$@XC-72/GCE sensor, and (b) bare GCE (i), UIO-66-NO$_2$/GCE sensor (ii), XC-72/GCE sensor (iii), and UIO-66-NO$_2$@XC-72/GCE sensor (iv). Supporting electrolyte: 0.1 M phosphate buffer solutions (PBS). Scan rate: 50 mV s^{-1} (pH 6.0).
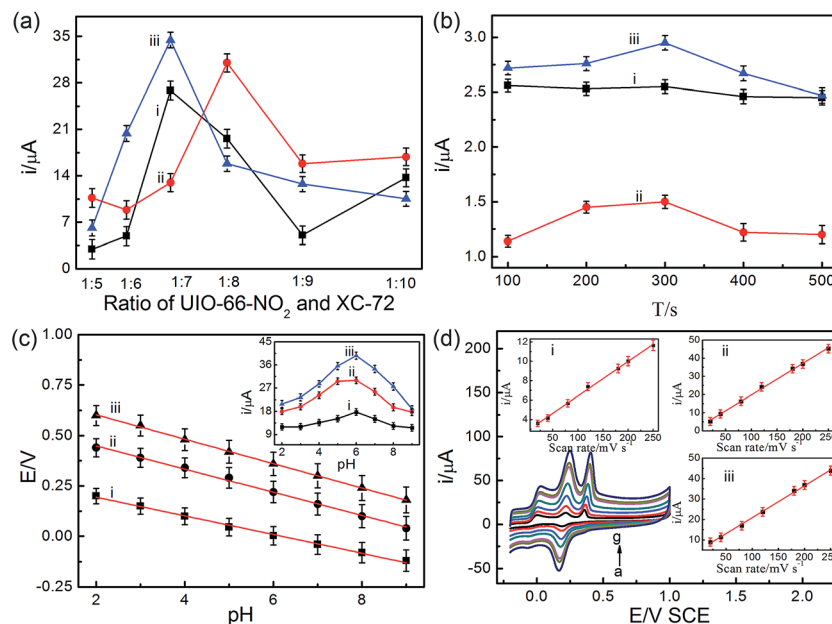

Fig. 4 Effects of the ratio of UIO-66-NO$_2$ and XC-72 (a), the accumulation time (b), pH value (c) and the scan rate (d) on the peak current for the oxidation of 3 μM AA (i), 1.5 μM DA (ii), and 1.5 μM UA (iii) in 0.1 M PBS at UIO-66-NO$_2$@XC-72/GCE sensor. Other conditions are the same as Fig. 3.

GCE sensor, the oxidation peaks of DA and UA at 0.2 V and 0.34 V suggested that the electroactive area of the electrode sensor increased significantly. Interestingly, there were obvious peaks of the three species at the UIO-66-NO$_2$@XC-72/GCE sensor, indicating high electrochemical activities in response to AA, DA and UA. The results demonstrated that the UIO-66-NO$_2$@XC-72/GCE sensor effectively facilitated the individual and simultaneous determination of the small biomolecules.

The experimental phenomena can be ascribed as follows: (i) XC-72 with high electrical conductivity can promote the electron transfer between modified electrode sensor surface and biomolecules, and enhance voltammetry peak separation. (ii) The UIO-66-NO$_2$@XC-72/GCE sensor possesses excellent electrochemical properties due to the synergetic effect of UIO-66-NO$_2$ and XC-72. (iii) The hydrogen bond between O (from –NO$_2$ group of UIO-66-NO$_2$) and H (from AA, DA and UA) can be helpful to improve the easy adsorption of AA, DA and UA, and finally promotes the response of the electrode sensor towards determination of the three biomolecules, especially contributes to the appearance of oxidation peak of AA (Scheme 1).

3.4 Optimization of the experimental conditions

To obtain the high sensitivity and selectivity, a series of optimized conditions were carried out in this paper. In this regard, the ratio of UIO-66-NO$_2$ and XC-72, the accumulation time, pH value and the scan rate were investigated. The effect factors were performed using CV method except for the accumulation time, which was employed DPV method.

The ratio of UIO-66-NO$_2$ and XC-72 plays important roles in the fabrication of the UIO-66-NO$_2$@XC-72/GCE sensor. It can be seen from Fig. 4a that the peak currents of AA and UA increased with the increasing ratio of the two materials until it obtained 1 : 7. Continuing increasing the ratio, the peak currents of the two materials until it obtained 1 : 7. Continuing increasing the ratio, the peak currents of the two biomolecules decreased sharply. For DA, the maximum of the peak current was achieved at the ratio of 1 : 8. The reason can be ascribed to the synergistic effect of the UIO-66-NO$_2$ and XC-72. The low ratio indicated the amount of XC-72 decreased, causing the conductivity of the fabricated sensor was poor and the electron transfer between the sensor and the analyte was impeded. By contrast, the high ratio meant the number of UIO-66-NO$_2$ decreased, the hydrogen bond between MOFs and the analyte was weaker and the surface area of the sensor became smaller. Based on the above experiments, the ratio of 1 : 7 was chosen for the following experiments.

From Fig. 4b, it was found that the accumulation time can affect the oxidation peak currents of the three biomolecules at the UIO-66-NO$_2$@XC-72/GCE sensor. The currents of DA and UA first increased and then decreased gradually with the increasing accumulation time, and the maximum value was 300 s. The current of AA nearly kept a constant with the change of the accumulation time. Therefore, 300 s was chosen in the following research for simultaneous determination of the three compounds.

It is well known that the pH value has a profound effect on the electrochemical response towards the determination of the analytes. From Fig. 4c, with the increase of pH from 2.0 to 9.0,

the oxidation potentials of the three biomolecules shifted negatively with linear slopes of 46.3, 57.5 and 60.6 mV per pH, respectively. The slopes were close to the theory value of 59 mV per pH, demonstrating that equal number of protons and electrons have taken part in the electrochemical redox reaction process.[53,54] It also can be seen that the peak currents of AA, DA and UA increased with the increasing pH value (from 2.0 to 6.0), and then it decreased from pH 6.0 to 9.0. In addition, the pK_a values of AA, DA and UA were 4.10, 8.87 and 5.75, respectively. DA existed as cationic species at pH 6.0. The carboxylic functional groups of MOFs at the electrode surface could effectively capture the cationic species.[3] However, AA and UA existed as unionized species at pH 6.0. In this case, the hydrogen bond effect between MOFs and the three biomolecules plays more important roles (Scheme 1). Therefore, 0.1 M PBS of pH 6.0 was selected as an optimized value for the further experiments.
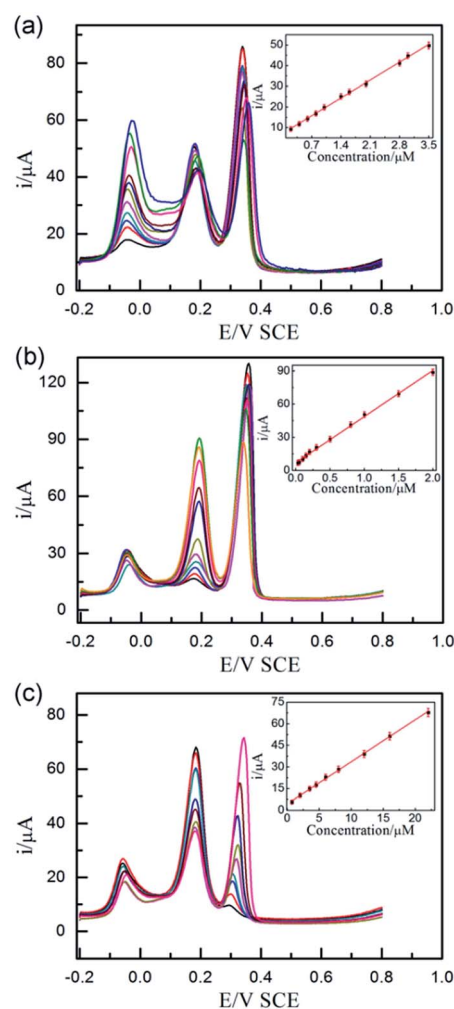

Fig. 5 DPVs of different concentrations of AA (a) (from inner to outer): 0.2, 0.4, 0.6, 0.8, 1.0, 1.4, 1.6, 2.0, 2.8, 3.0, 3.5 μM containing 1.5 μM DA, 1.5 μM UA, different concentrations of DA (b) (from inner to outer): 0.03, 0.05, 0.1, 0.15, 0.2, 0.3, 0.5, 0.8, 1.0, 1.5, 2.0 μM containing 3 μM AA, 1.5 μM UA, and different concentrations of UA (c) (from inner to outer): 0.75, 2.0, 3.5, 4.5, 6.0, 8.0, 12, 16, 22 μM containing 3 μM AA, 1.5 μM DA at UIO-66-NO$_2$@XC-72/GCE sensor. Other conditions are the same as Fig. 3. The inset figures show the plots of the peak currents vs. the concentration of AA, DA and UA, respectively.

Table 2 Comparison of the optimized sensors for the detection of AA, DA and UA with other modified electrode sensors

Methods	Linear range (µM)			Detection limit (µM)			References
	AA	DA	UA	AA	DA	UA	
DpAu/PTCA-Cys/GCE	20–700	2–402	0.4–252	6.40	0.67	0.12	3
Carbon nanotube/GCE	80–1360	0.5–10	—	20	0.10	—	10
Au/RGO/GCE	240–1500	6.8–41	8.8–53	51	1.40	1.80	13
*Polymer/GCE[a]	150–1000	0.1–200	10–130	10	0.02	1.00	18
P-ATD/GCE	30–300	5–50	10–100	2.01	0.33	0.19	19
NCNF/GCE	50–3000	1–200	5.0–200	50	0.50	1.00	49
NiCo-NPs-in-N/C	500–1500	0.5–900	10–500	0.09	0.08	0.01	47
rGO–CNT/ITO	10–200	0.2–8.0	0.2–16	5.31	0.04	0.17	55
SZP/MB	100–1600	6–100	22–350	8.30	1.70	3.70	57
GEF/CFE	74–2306	1.4–125.7	4.0–371	73.52	1.36	3.98	56
This work	0.2–3.5	0.03–2.0	0.8–22	0.12	0.005	0.03	

[a] *Polymer represents poly(eriochrome black T).

Table 3 Recoveries of the determination of DA and UA in the real samples

Samples	Detected (µM)	Added (µM)	Found (µM)	Recovery (%)	RSD (%) ($n = 3$)
Injection		10	38.40	101.3	1.38
Solution	27.90	15	43.10	100.5	1.96
(DA)		20	47.10	98.3	1.52
Urine	13.87	10	24.12	101.0	1.75
(UA)		20	34.09	100.7	2.32
		35	48.47	99.2	1.94

To evaluate the reaction kinetics, the CV responses at different scan rates for the three compounds was investigated. Fig. 4d shows that the oxidation peak currents of AA, DA and UA gradually increased as the scan rate increases, with a linear relationship between the peak currents and the scan rate in the range of 20–250 mV s^{-1} (the inset of Fig. 4d). The regression equations were expressed as follows I_{AA} (µA) = 2.86 + 0.036C_{AA} (µM) ($R^2 = 0.998$), I_{DA} (µA) = 2.32 + 0.17C_{DA} (µM) ($R^2 = 0.998$) and I_{UA} (µA) = 5.26 + 0.16C_{UA} (µM) ($R^2 = 0.998$). It demonstrates that electrochemical reaction of the three biomolecules at UIO-66-NO$_2$@XC-72/GCE sensor was a surface-controlled process.

3.5 Simultaneous determination of AA, DA and UA

Fig. 5 displays DPV responses of the mixture of AA, DA and UA when the concentration of the detected analyte changed with the other two species keeping constant at the optimized electrode sensor. The experiments indicated the UIO-66-NO$_2$@XC-72/GCE sensor exhibited wide linear relationships between the oxidation peak current responses and the analytes concentrations, with the correlation coefficient of 0.998, 0.998 and 0.999, respectively. The following linear regression equations were expressed as I_{AA} (µA) = 7.08 + 12.35C_{AA} (µM), I_{DA} (µA) = 6.90 + 41.81C_{DA} (µM) and I_{UA} (µA) = 4.34 + 2.93C_{UA} (µM). The detection ranges were 0.2–3.5 µM for AA, 0.03–2.0 µM for DA and 0.75–22 µM for UA with the detection limits were 0.12, 0.005 and 0.03 µM (S/N = 3), respectively.

The performance of the UIO-66-NO$_2$@XC-72/GCE senor was compared with some existing sensors, as shown in Table 2. The minimum concentrations of AA, DA and UA and the detection limits of this paper are lower than that of those previously reported materials.[3,10,13,18,19,47,49,55–57] These results confirmed that the UIO-66-NO$_2$@XC-72 material was a promising material for the electroanalytical detection of the three biomolecules.

3.6 Reproducibility and stability

The reproducibility of the UIO-66-NO$_2$@XC-72/GCE sensor was evaluated. The relative standard deviations (RSD) for five different electrode sensors were 5.04% for AA, 4.08% for DA and 4.92% for UA. The RSD of the same sensor in eight successive experiments were 3.02% for AA, 2.54% for DA and 2.92% for UA, suggesting the proposed sensor exhibited excellent reproducibility. Furthermore, the sensor was stored in the refrigerator at 4 °C. After 10 days, there was only an 8% loss in the response current of the developed sensor. After 30 days, the proposed sensor can retain 85% of its initial response, which was stable enough for the application in electrochemical sensor.

3.7 Real sample analysis

The proposed method was evaluated for the determination of AA, DA and UA in the real samples. DA hydrochloride injection solution and human urine were measured for analysis. Generally, DA and UA samples were diluted 10 times and 100 times with PBS, respectively. The spiked sample with certain amounts of DA and UA were added to the corresponding samples. Subsequently, the experiments were carried out five times and the Table 3 summarized the analytical results. It can be seen that the RSD is in the range of 1.38–2.32% and the recovery is between 98.3–101.3%. It indicated that the proposed sensor possessed sufficient precision and high accuracy.

4. Conclusions

In conclusion, a new approach for fabrication of the UIO-66-NO$_2$@XC-72/GCE sensor was presented for the first time to

simultaneously determine AA, DA and UA. The procedure of fabricating sensor was simple, convenient and rapid. The developed sensor exhibited high sensitivity and selectivity with wide linear concentration range and low detection limit. Interestingly, the satisfactory results indicate that MOFs could be a promising candidate for application in electroanalysis, and promisingly, it was used by mixing with other conductive materials to fabricate excellent sensors to detect other electrochemical biomolecules.

Acknowledgements

References

1 A. A. Abdelwahab and Y.-B. Shim, *Sens. Actuators, B*, 2015, **221**, 659–665.

2 M. Noroozifar, M. Khorasani-Motlagh, R. Akbari and M. Bemanadi Parizi, *Biosens. Bioelectron.*, 2011, **28**, 56–63.

3 W. Zhang, Y. Chai, R. Yuan, J. Han and S. Chen, *Sens. Actuators, B*, 2013, **183**, 157–162.

4 Y. J. Yang and W. Li, *Biosens. Bioelectron.*, 2014, **56**, 300–306.

5 L. Zhao, H. Li, S. Gao, M. Li, S. Xu, C. Li, W. Guo, C. Qu and B. Yang, *Electrochim. Acta*, 2015, **168**, 191–198.

6 M. Behpour, S. M. Ghoreishi, E. Honarmand and M. Salavati-Niasari, *Analyst*, 2011, **136**, 1979–1986.

7 D. Datta, R. K. Bera, S. Jana, B. Manna, D. Roy, A. Anoop, C. R. Raj and T. Pathak, *Chem.–Asian J.*, 2015, **10**, 1554–1560.

8 Z. Yang, X. Zheng, Z. Li and J. Zheng, *Analyst*, 2016, **141**, 4757–4765.

9 N. Jia, Z. Wang, G. Yang, H. Shen and L. Zhu, *Electrochem. Commun.*, 2007, **9**, 233–238.

10 Z. Wang, J. Liu, Q. Liang, Y. Wang and G. Luo, *Analyst*, 2002, **127**, 653–658.

11 Z. Wang, M. Shoji and H. Ogata, *Analyst*, 2011, **136**, 4903–4905.

12 W. A. El-Said, J.-H. Lee, B.-K. Oh and J.-W. Choi, *Electrochem. Commun.*, 2010, **12**, 1756–1759.

13 C. Wang, J. Du, H. Wang, C. E. Zou, F. Jiang, P. Yang and Y. Du, *Sens. Actuators, B*, 2014, **204**, 302–309.

14 Y. Temerk and H. Ibrahim, *Sens. Actuators, B*, 2016, **224**, 868–877.

15 L. X. Chen, J. N. Zheng, A. J. Wang, L. J. Wu, J. R. Chen and J. J. Feng, *Analyst*, 2015, **140**, 3183–3192.

16 S. Mahshid, C. Li, S. S. Mahshid, M. Askari, A. Dolati, L. Yang, S. Luo and Q. Cai, *Analyst*, 2011, **136**, 2322–2329.

17 J. Bai, B. Lu, X. Bo and L. Guo, *Electrochem. Commun.*, 2010, **12**, 1563–1567.

18 H. Yao, Y. Sun, X. Lin, Y. Tang and L. Huang, *Electrochim. Acta*, 2007, **52**, 6165–6171.

19 P. Kalimuthu and S. A. John, *Talanta*, 2010, **80**, 1686–1691.

20 M. Pandurangachar, B. E. Kumara Swamy, B. N. Chandrashekar, O. Gilbert and B. S. Sherigara, *J. Mol. Liq.*, 2011, **158**, 13–17.

21 X. Jiang and X. Lin, *Analyst*, 2005, **130**, 391–396.

22 K. Deng, J. Zhou and X. Li, *Electrochim. Acta*, 2013, **114**, 341–346.

23 S. Yu, C. Luo, L. Wang, H. Peng and Z. Zhu, *Analyst*, 2013, **138**, 1149–1155.

24 M. Kandiah, M. H. Nilsen, S. Usseglio, S. Jakobsen, U. Olsbye, M. Tilset, C. Larabi, E. A. Quadrelli, F. Bonino and K. P. Lillerud, *Chem. Mater.*, 2010, **22**, 6632–6640.

25 S. S. Nagarkar, A. V. Desai and S. K. Ghosh, *Chemistry*, 2015, **21**, 9994–9997.

26 Y. Bai, Y. Dou, L. H. Xie, W. Rutledge, J. R. Li and H. C. Zhou, *Chem. Soc. Rev.*, 2016, **45**, 2327–2367.

27 S. Han, S. C. Warren, S. M. Yoon, C. D. Malliakas, X. Hou, Y. Wei, M. G. Kanatzidis and B. A. Grzybowski, *J. Am. Chem. Soc.*, 2015, **137**, 8169–8175.

28 C. Hou, Y. L. Bai, X. Bao, L. Xu, R. G. Lin, S. Zhu, J. Fang and J. Xu, *Dalton Trans.*, 2015, **44**, 7770–7773.

29 X. L. Hu, F. H. Liu, C. Qin, K. Z. Shao and Z. M. Su, *Dalton Trans.*, 2015, **44**, 7822–7827.

30 S. J. Garibay and S. M. Cohen, *Chem. Commun.*, 2010, **46**, 7700–7702.

31 S. Dang, T. Wang, F. Yi, Q. Liu, W. Yang and Z. M. Sun, *Chem.–Asian J.*, 2015, **10**, 1703–1709.

32 Y. Fang, S. Guo, C. Zhu, S. Dong and E. Wang, *Chem.–Asian J.*, 2010, **5**, 1838–1845.

33 Y. Kobayashi, B. Jacobs, M. D. Allendorf and J. R. Long, *Chem. Mater.*, 2010, **22**, 4120–4122.

34 T. C. Narayan, T. Miyakai, S. Seki and M. Dinca, *J. Am. Chem. Soc.*, 2012, **134**, 12932–12935.

35 Y. Li, C. Huangfu, H. Du, W. Liu, Y. Li and J. Ye, *J. Electroanal. Chem.*, 2013, **709**, 65–69.

36 A. A. Talin, A. Centrone, A. C. Ford, M. E. Foster, V. Stavila, P. Haney, R. A. Kinney, V. Szalai, F. El Gabaly, H. P. Yoon, F. Leonard and M. D. Allendorf, *Science*, 2014, **343**, 66–69.

37 B. Le Ouay, M. Boudot, T. Kitao, T. Yanagida, S. Kitagawa and T. Uemura, *J. Am. Chem. Soc.*, 2016, **138**, 10088–10091.

38 F. Ragon, B. Campo, Q. Yang, C. Martineau, A. D. Wiersum, A. Lago, V. Guillerm, C. Hemsley, J. F. Eubank, M. Vishnuvarthan, F. Taulelle, P. Horcajada, A. Vimont, P. L. Llewellyn, M. Daturi, S. Devautour-Vinot, G. Maurin, C. Serre, T. Devic and G. Clet, *J. Mater. Chem. A*, 2015, **3**, 3294–3309.

39 X. Zhao, X. Liu, Z. Zhang, X. Liu and W. Zhang, *RSC Adv.*, 2016, **6**, 92011–92019.

40 S. Ling and B. Slater, *Chem. Sci.*, 2016, **7**, 4706–4712.

41 E. A. Kozlova, V. N. Panchenko, Z. Hasan, N. A. Khan, M. N. Timofeeva and S. H. Jhung, *Catal. Today*, 2016, **266**, 136–143.

42 V. N. Panchenko, M. N. Timofeeva and S. H. Jhung, *Catal. Rev.*, 2016, **58**, 209–307.

43 J. Hu, H.-B. Zhang, S. Hong, Z.-G. Jiang, C. Gui, X. Li and Z.-Z. Yu, *Ind. Eng. Chem. Res.*, 2014, **53**, 2270–2276.

44 W. W. Zhao, C. Y. Zhang, Z. G. Yan, L. P. Bai, X. Wang, H. Huang, Y. Y. Zhou, Y. Xie, F. S. Li and J. R. Li, *J. Chromatogr. A*, 2014, **1370**, 121–128.

45 X. Ren, D. Shao, S. Yang, J. Hu, G. Sheng, X. Tan and X. Wang, *Chem. Eng. J.*, 2011, **170**, 170–177.

46 Y. Huang, W. Qin, Z. Li and Y. Li, *Dalton Trans.*, 2012, **41**, 9283–9285.

47 X. Zhang, W. Yan, J. Zhang, Y. Li, W. Tang and Q. Xu, *RSC Adv.*, 2015, **5**, 65532–65539.

48 Z. Xue, Y. Feng, H. Guo, C. Hu, A. Mahmoud idris Mohmed, J. Li and X. Lu, *RSC Adv.*, 2014, **4**, 5849.

49 J. Sun, L. Li, X. Zhang, D. Liu, S. Lv, D. Zhu, T. Wu and T. You, *RSC Adv.*, 2015, **5**, 11925–11932.

50 H. Imran, P. N. Manikandan and V. Dharuman, *RSC Adv.*, 2015, **5**, 63513–63520.

51 H. L. Poh and M. Pumera, *Chem.–Asian J.*, 2012, **7**, 412–416.

52 L. Zhang, L. Ning, S. Li, H. Pang, Z. Zhang, H. Ma and H. Yan, *RSC Adv.*, 2016, **6**, 66468–66476.

53 F. Ye, C. Feng, J. Jiang and S. Han, *Electrochim. Acta*, 2015, **182**, 935–945.

54 X. Zhang, L.-X. Ma and Y.-C. Zhang, *Electrochim. Acta*, 2015, **177**, 118–127.

55 Y. Zhang, Y. Ji, Z. Wang, S. Liu and T. Zhang, *RSC Adv.*, 2015, **5**, 106307–106314.

56 J. Du, R. Yue, F. Ren, Z. Yao, F. Jiang, P. Yang and Y. Du, *Biosens. Bioelectron.*, 2014, **53**, 220–224.

57 J. Argüello, V. L. Leidens, H. A. Magosso, R. R. Ramos and Y. Gushikem, *Electrochim. Acta*, 2008, **54**, 560–565.